

University of Louisville

## ThinkIR: The University of Louisville's Institutional Repository

---

Electronic Theses and Dissertations

---

12-2021

### Atomistic investigation of phase stability and sodium ion conduction in sulfide electrolytes.

Sabina Zakhidovna Chertmanova

Follow this and additional works at: <https://ir.library.louisville.edu/etd>



Part of the [Energy Systems Commons](#)

---

#### Recommended Citation

Chertmanova, Sabina Zakhidovna, "Atomistic investigation of phase stability and sodium ion conduction in sulfide electrolytes." (2021). *Electronic Theses and Dissertations*. Paper 3798.

<https://doi.org/10.18297/etd/3798>

This Master's Thesis is brought to you for free and open access by ThinkIR: The University of Louisville's Institutional Repository. It has been accepted for inclusion in Electronic Theses and Dissertations by an authorized administrator of ThinkIR: The University of Louisville's Institutional Repository. This title appears here courtesy of the author, who has retained all other copyrights. For more information, please contact [thinkir@louisville.edu](mailto:thinkir@louisville.edu).

ATOMISTIC INVESTIGATION OF PHASE STABILITY AND SODIUM ION  
CONDUCTION IN SULFIDE ELECTROLYTES

By

Sabina Zakhidovna Chertmanova  
B.S., University of Louisville, 2020  
M.S., University of Louisville, 2021

A Thesis  
Submitted to the Faculty of the  
J.B. Speed School of Engineering of the University of Louisville  
in Partial Fulfillment of the Requirements  
for the Degree of

Master of Science in Mechanical Engineering

Department of Mechanical Engineering  
University of Louisville  
Louisville, Kentucky

December 2021

Copyright 2021 by Sabina Zakhidovna Chertmanova

All rights reserved



ATOMISTIC INVESTIGATION OF PHASE STABILITY AND SODIUM ION  
CONDUCTION IN SULFIDE ELECTROLYTES

By

Sabina Zakhidovna Chertmanova  
B.S., University of Louisville, 2020  
M.S., University of Louisville, 2021

A Thesis Approved on

December 1, 2021

by the following Thesis Committee:

---

Narayanan, Badri

---

Wang, Hui

---

Sumanasekera, Gamini U.

## DEDICATION

This thesis is dedicated to my parents.

## ACKNOWLEDGMENTS

I would like to thank my thesis adviser, Dr. Badri Narayanan, for his guidance and patience. I would also like to thank the other committee members, Dr. Hui Wang and Dr., Gamini U. Sumanasekera, for their comments and assistance. I would also like to express my gratitude to my husband, Mahad Mohamed, for his tremendous support and patience through the process. Last, but not least, I would like to thank my parents, Sureya Ashraf and Zakhid Chertmanov, who uprooted and immigrated to the U.S.A. to give their children a better chance of pursuing education.

## ABSTRACT

### ATOMISTIC INVESTIGATION OF PHASE STABILITY AND SODIUM ION CONDUCTION IN SULFIDE ELECTROLYTES

Sabina Zakhidovna Chertmanova

December 1, 2021

In this thesis, we employ a combination of density functional theory (DFT) calculations, and *ab initio* molecular dynamics (AIMD) simulations to identify the effect of chemical doping on (a) thermodynamic phase stability, and (b) Na-ion conduction in  $\text{Na}_3\text{SbS}_4$  (NSS) solid-state electrolytes. We found that (a) Se doped electrolytes, namely,  $\text{Na}_3\text{SbSe}_x\text{S}_{4-x}$  undergo a tetragonal-to-cubic structural phase transition at  $x > 3$  (Se-rich), and (b) the size, valence, and electronegativity of chemical dopants that substitute Na in  $\text{Na}_3\text{SbS}_4$  have a cumulative profound impact on Na-ion conductivity. Specifically, substituting Na with higher valence dopant (e.g.,  $\text{In}^{3+}$ ) that are similar in size to Na can result in substantial improvement in Na-ion conduction (~2-2.5 times that in undoped case) owing to the increased Na-vacancy concentration in the doped electrolytes. AIMD trajectories also elucidate the effect of dopant on the atomic-scale pathways underlying Na-conduction.

## TABLE OF CONTENTS

ACKNOWLEDGMENTS .....	iv
ABSTRACT.....	v
LIST OF FIGURES .....	vii
INTRODUCTION .....	1
BACKGROUND .....	4
COMPUTATIONAL METHODS.....	7
PHASE STABILITY OF SELENIUM-DOPED SULFIDE ELECTROLYTE.....	11
EFFECT OF CHEMICAL DOPING ON SODIUM ION CONDUCTION.....	16
CONCLUSIONS.....	40
REFERENCES .....	41
APPENDIX.....	44
CURRICULUM VITA .....	46

## LIST OF FIGURES

FIGURE	PAGE
Figure 1. Cohesive energy data points found in all possible combinations of sites that Se can substitute S atoms with $x=4$ in $c\text{-Na}_6\text{Sb}_2\text{S}_{8-x}\text{Se}_x$ and $t\text{-Na}_6\text{Sb}_2\text{S}_{8-x}\text{Se}_x$ .	13
Figure 2. Difference in energies between cubic and tetragonal phases at various levels of Se doping ( $x$ ).	14
Figure 3. Planar differences in between undoped NSS and single Se-doped NSS in (a-b) Cubic, (c-d) Tetragonal phases.	15
Figure 4. plot of MSD vs. simulation time of c-Ga-doped NSS from 800K-1200K obtained from trajectory files.	17
Figure 5. Arrhenius plot of diffusivity for cubic structures.	19
Figure 6. Arrhenius plot of diffusivity for tetragonal structures.	20
Figure 7. Comparison amongst each composition, polymorph, and corresponding activation energy.	21
Figure 8. Comparison amongst each composition, polymorph, and corresponding pre-exponential factor.	22
Figure 9. Comparison amongst each composition, polymorph, and corresponding formation energies.	25
Figure 10. Ball-and-stick simulation model supercell of c-Based in (a) Top view, (b) Isometric view. Sodium ions, sulfur ions, and antimony ions are seen as purple, blue, and yellow atoms, respectively.	26
Figure 11. Ball-and-stick simulation model supercell of t-Based in (a) Top view, (b) Isometric view. Sodium ions, sulfur ions, and antimony ions are seen as purple, blue, and yellow atoms, respectively.	27
Figure 12. A small portion of sodium diffusion pathways assessed in c-Base at (a) 900 K, (b) 1200 K, via the selection and tracking of same Na ion.	28
Figure 13. Ball-and-stick visual comparison of (a) c-Base, undoped NSS and (b) c-Ba-doped NSS, and the interaction between $\text{SbS}_4$ tetrahedron (Sb ions seen in yellow, S ions in blue) and Na-Na ion (purple)/Ba ion (green)-Na ion interactions at 1200 K.	32

Figure 14. Ball-and-stick visual representation of c-Ga-doped NSS and the (a) interaction between  $\text{Na}^+$  ion and Ga dopant and (b) corresponding visual images of overall structure and sites that Na occupies, at 1200 K. 33

Figure 15. Ball-and-stick visual representation of c-Ba-doped NSS and the (a) interaction between  $\text{Na}^+$  ion and Ba dopant and (b) corresponding visual images of overall structure and sites that Na occupies, at 1200 K. 34

Figure 16. Ball-and-stick visual representation of c-In-doped NSS and the (a) interaction between  $\text{Na}^+$  ion and In dopant and (b) corresponding visual images of overall structure and sites that Na occupies, at 1200 K. 35

Figure 17. Ball-and-stick visual representation of t-Ga-doped NSS and the (a) interaction between  $\text{Na}^+$  ion and Ga dopant and (b) corresponding visual images of overall structure and sites that Na occupies, at 1200 K. 36

## CHAPTER I

### INTRODUCTION

As environmental issues increase due to conventional methods of energy supply, society is at search for alternative methods of energy, such as wind and solar power. This in turn, raises the need for alternative energy storage solutions. For decades Lithium-ion batteries (LIBs) have been the main player as an energy storage solution from consumer electronics, such as kid's toys, phones, and laptops, to electric vehicles, aerospace industry, and grid storage. This is thanks to large efforts in battery research developments that have led to improved performance and reduced production costs. However, with increasing market price of lithium (Li) and safety hazards, such as battery fires and explosions, that come with batteries containing liquid organic electrolytes like LIBs, efforts are being made to find an efficient, safe, and abundant replacement.

Consequently, one of the attractive alternatives to energy storage has been all-solid-state batteries (ASSBs) due to the elimination of liquid electrolytes from batteries altogether and thus, relies on the use of inorganic solid state electrolytes (SSEs). ASSBs are projected to be the future of batteries as they have noncombustible solid electrolytes (SEs), improve energy density and recyclability, can operate at room temperature, and have wide operating temperature range which reduces the need for cooling power requirements. Many of ASSBs characteristics allow for energy efficiency, consumer safety, and cost

reduction during manufacturing phase, consuming phase, and the afterlife of the battery. Sodium-ion batteries (NIBs) are favorable candidates for ASSBs as sodium (Na) based on its standard potential, naturally abundant – 1,180 times the available supply of Li and has similar battery chemistry to Li batteries. Though NIBs were first developed in the 1970s, in use with liquid organic electrolytes, their poor performance compared to LIBs hindered their utilization and limited the number of studies conducted in this area, thus, leading to gaps in literature of NIBs that still need to be understood. However, in combination with SSE, NIBs have gained interest in the battery research field. The NIBs are evaluated on various levels such as its ionic conductivity, mechanical strength, interfacial contact, electrochemical stability, thermal stability, and ease of production.

Going more into details of NIBs, one of the first major NIB findings consist of  $\beta''$ - $\text{Al}_2\text{O}_3$  which was reported to have ionic conductivity of  $1 \times 10^{-3}$  S/cm [1]. Only two decades after,  $\text{Na}_3\text{Zr}_2\text{Si}_2\text{PO}_{12}$  was reported to exhibit higher conductivity than that of a popular lithium ion electrolyte,  $\text{Li}_{1.3}\text{Al}_{0.3}\text{Ti}_{1.7}(\text{PO}_4)_3$  [2]. Since lithium ion batteries took primary stance in electrochemical storage systems, there was sort of a pause in NIB research that resumed around 2010's one of which, Wang et al. conducted on solid  $\text{Na}_3\text{PS}_4$  (NPS), discovering conductivity of  $2 \times 10^{-4}$  S/cm at room temperature [3]. This study jumpstarted many studies to be centered around solid sodium ion electrolytes. The following studies consisted of variations of the NPS compound such as  $\text{Na}_4\text{SiS}_4$ ,  $\text{Na}_3\text{PSe}_4$ ,  $\text{Na}_3\text{SbSe}_4$ ,  $\text{Na}_{11}\text{Sn}_2\text{PS}_{12}$ ,  $\text{Na}_{2.730}\text{Ca}_{0.135}\text{PS}_4$ ,  $t\text{-Na}_{2.9375}\text{PS}_{3.9375}\text{Cl}_{0.0625}$ ,  $\text{Na}_3\text{SbS}_4$ ,  $\text{Na}_{2.88}\text{Sb}_{0.88}\text{W}_{0.12}\text{S}_4$ , reporting comparable room temperature ionic conductivities in the ranges of  $7.4 \times 10^{-4}$  -  $3.2 \times 10^{-2}$  S/cm [4, 13].

Furthermore, sulfide-based SEs, though said to have low air stability, have also attracted attention due to their mechanical properties and chemical stability. This includes benefits of wide electrochemical window, high conductivity, and desired mechanical properties in ASSBs such as a high elastic modulus [14]. Thus, exploration of sodium-sulfur solid electrolytes such as  $\text{Na}_3\text{SbS}_4$ , has taken front row seat in NIBs research as NSS has been used as a base compound for various interfacial and ionic conductivity studies. As the search for a composition that contains the desirable traits mentioned above continues, areas of research use various methods to increase ionic conductivity of NSS electrolytes.

For the first portion of this thesis, DFT will be used to look into phase stability of Selenium-doped sulfur in NSS since often, the cubic crystal structure of NSS is found to have desirable conduction traits. While the lack of studies and understanding found for NIBs and effects of different temperature ranges, dopant elements' ionic radius and electronegativity is a motivator for the second portion of this thesis where DFT and AIMD, will be used to study  $\text{Na}_6\text{Sb}_2\text{S}_8$ , in its cubic and tetragonal polymorphs and the effects various doping elements via substitutional doping, of differing ionic radii, number of valence electrons, electronegativity, and high temperatures have on  $\text{Na}^+$  diffusivity,  $\text{Na}^+$  ion activation energy barrier, formation energy and ionic conductivity.

## CHAPTER II

### BACKGROUND

Firstly, there are many advantages in using chalcogenides in SSEs, as a comparison to oxide-based SSEs, which can have poor interfacial stability due to dendrite formation and is often unstable with cathode materials, chalcogenides, such as sulfides or selenides offer larger ionic radii and lower electronegativity, presenting a weaker bonding strength between the chalcogenide and cation, ( $\text{Na}^+$ ) element [15]. This weakened bond allows for better mobility within sodium-ion transport.

$\text{Na}_3\text{SbS}_4$  is like  $\text{Na}_3\text{PS}_4$  conductor, in that it also displays polymorphs that include tetragonal structure (F43 space group) at room temperature and cubic structure (P421c space group) at elevated temperatures [20-21]. For  $\text{Na}_3\text{SbS}_{4-x}\text{Se}_x$  conductors, the partial replacement of S by large anion Se only changes its crystal structure but also enhance the ionic conductivity by reducing grain boundary resistance [22-23]. The feasibility of  $\text{Na}_3\text{SbS}_4$  and  $\text{Na}_3\text{SbS}_x\text{Se}_{4-x}$  SSEs is demonstrated in solid-state Na batteries pairing with various cathodes (e.g.,  $\text{FeS}_2$ ,  $\text{TiS}_2$ , etc.) [20, 23-25].

Since the second portion of this thesis focuses on sodium ion conduction, the main interest lies in characteristics of NIBs and ways to greatly improve Na diffusivity. There are various methods of increasing Na ion diffusion a few of which include interstitial doping, substitutional doping, introduction of vacancies, systematic changes

such as increase of temperature, and structural optimization such as micro-scaled 3D diffusion pathways through specific synthesis methods [18]. Substitutional doping, which will be implemented in this study, has numerous effects on the crystal structure, diffusion pathways, activation energy, formation energy, and introduction of vacancies.

To further elaborate, the extent and type of influence that substitutional doping has largely relies on the dopant element itself. The ionic charge, its radii, the concentration of the dopant. Aliovalent substitutions is where the doping element has a differing charge when compared to the element that is being substituted. For example, in this study, the element being substituted is the cation  $\text{Na}^+$ , meanwhile, dopant atoms include elements from Groups 2, 3, and 13 and have double or triple the ionic charge of the sodium ion. This results in more sodium ions being removed than the number of dopants being substituted in, yielding vacancies in the lattice when an  $\text{Na}^+$  ion once resided. This is an important byproduct of aliovalent doping as it creates a site where sodium ions can hop to, which in turn increases diffusion. Though vacancies can be induced through, they are not limited to aliovalent substitutions and can be introduced without any dopants.

Some previous work which shows the impact of vacancies in doped and undoped cases include a computational study where increasing vacancy concentration to only 2% in  $\text{Na}_3\text{PS}_4$  was found to enhance conductivity by one order of magnitude, while Chu et al. found in experimental study that  $t\text{-Na}_{3-x}\text{PS}_{4-x}\text{Cl}_x$  with  $x=0.0625$  resulted in a conductivity of 1.14 mS/cm at room temperature, (RT) [19,9]. Furthermore, in a study of  $\text{Na}_{10+x}\text{Sn}_{1+x}\text{P}_{2-x}\text{S}_{12}$ , Duchardt et al. display the importance of vacancy and its effects on  $\text{Na}^+$  conduction by showing that due to vacancy formations, at  $x=1$ ,  $\text{Na}_{11}\text{Sn}_2\text{PS}_{12}$  yields

an ionic conductivity of  $3.7 \pm 0.3$  mS/cm [7]. This is further confirmed in  $\text{Na}_3\text{SbS}_4$  computational study by Jalem et al. where in undoped cases, extrapolation of data to RT shows 8.280 mS/cm and 21.98 mS/cm at 2% and 4% Na vacancy concentration, respectively. Meanwhile, in cases where Antimony (Sb) was doped with Molybdenum (Mo) and Tungsten (W) and a 4% Na vacancy concentration was present, maximum ionic conductivity of 44.94 mS/cm and 80.63 mS/cm respectively, was found at RT [16].

Furthermore, the ionic charge, or oxidation state of the dopant element, specifically in comparison to the element that it is substituting. This is likely due to the interaction that will take place between same charge species in the lattice. For example, if  $\text{Na}^+$  ion is being substituted with another cation of oxidation state 1+, then it is most likely not going to make much difference to sodium diffusion compared to if there is aliovalent substitution by an element with higher oxidation state. With a higher charged doping ion, there will likely be increased coulombic repulsion between the doping ion and sodium ions within nearby sites. Thus, more of an influence for sodium ions to jump and increase diffusivity. This will also in turn, influence activation and formation energies found in doped compositions.

Lastly, an impedance to sodium diffusion can be caused by pathway bottleneck areas within to the crystal structure usually created by the volume  $\text{SbS}_4$  tetrahedral takes up in the crystal structure which tends to block the channels which  $\text{Na}^+$  ion would like to travel through. This consists of a pathway described by the diameter known as bottleneck diameter. The study by Jalem et al. also showed enhanced 3D diffusion pathways due to dopant ions as they tend to induce larger Na Wyckoff site cages due to smaller  $\text{WS}_4/\text{MoS}_4$  tetrahedral volume relative to  $\text{SbS}_4$  [16].

## CHAPTER III

### COMPUTATIONAL METHODS

To understand phase stability in selenium doped NSS, first principles calculations based on DFT were performed via Vienna ab initio simulation package (VASP). The exchange-correlation energy was treated with the generalized gradient approximation (GGA), using the functional of Perdew-Burke-Ernzerhof (PBE).  $2 \times 1 \times 1$  supercells of the unit cells c- $\text{Na}_3\text{SbS}_4$  and t- $\text{Na}_3\text{SbS}_4$  were created to obtain the model cells and incorporate the Se substitution, c- $\text{Na}_6\text{Sb}_2\text{S}_{8-x}\text{Se}_x$  and t- $\text{Na}_6\text{Sb}_2\text{S}_{8-x}\text{Se}_x$ , respectively. The simulation process for both polymorphs were the same, in the first step, the cell was allowed to adjust its volume and relax around the new size of the Se atom by setting ISIF to 7 while forces and stress tensors were calculated, next ISIF was set to 2 to allow ionic movement to allow energy optimization, this is also known as the utilization of the Nose-Hoover thermostat (NVT ensemble).

For both steps, the kinetic energy cutoff was set to 520 eV, temperature of the system was assumed 0 K, and the number of maximum ionic steps to be taken was limited to 99. The structures were optimized with the conjugate gradient method, energy convergence value between consecutive steps was set to  $10^{-6}$  eV and lastly,  $\Gamma$ -centered  $3 \times 3 \times 3$  k-point mesh was adopted.

For observation of the effects of various chemical doping elements in NSS for sodium ion conduction, first, using DFT, the first principles calculations were performed on the unit cells, c-Na<sub>6</sub>Sb<sub>2</sub>S<sub>8</sub> and t-Na<sub>6</sub>Sb<sub>2</sub>S<sub>8</sub>, via VASP, in which, the exchange-correlation energy was treated with the GGA using the functional of PBE. Relaxation of the unit cell was performed in the same manner as the DFT calculations of selenide doped NSS.

A  $2 \times 2 \times 1$  supercell was then created to obtain c-Na<sub>24</sub>Sb<sub>8</sub>S<sub>32</sub> and t-Na<sub>24</sub>Sb<sub>8</sub>S<sub>32</sub> and the dopant elements, Ca<sup>2+</sup>, Ba<sup>2+</sup>, In<sup>3+</sup>, Y<sup>3+</sup>, and Ga<sup>3+</sup>, were incorporated to create model supercells to be used in AIMD calculations, these compositions can be found in Table 1. The step size for the molecular dynamics (MD), was set to 1 fs and an energy cutoff of 336 eV was used for model cells containing Ba<sup>2+</sup>, In<sup>3+</sup>, Y<sup>3+</sup>, and Ga<sup>3+</sup> dopants and 346 eV for those that are Ca<sup>2+</sup> doped. A Monkhorst-pack k-point scheme of  $1 \times 1 \times 1$  was implemented, and the pseudopotentials used for all participating elements were of standard forms. The target temperatures were set between 800 K and 1200 K with increments of 100 K. The trajectory sampling was carried out for 100,000 steps with a NVT ensemble. All 60 possible combinations of cell structure, compositions, and temperatures were generated and used in the AIMD simulations.

The Ca-doped and Ba-doped model cell compositions shown in Table 1 results in single sodium ion vacancy, while the Ga-doped, In-doped, and Y-doped results in two Na<sup>+</sup> ion vacancies.

Lastly, with the goal of finding formation energies associated with each composition,  $E_{form_{composition}}$ , created, further relaxations were performed for each model

supercells, both cubic and tetragonal, and for each element's most stable crystalline structures. These relaxations consisted of the same method utilized in the DFT calculations of selenide doped NSS, with the exception of utilization of ISIF 3 in this case for allowance of degrees of freedom such as cell shape, volume, and atom positions, in these relaxations.

**Table 1**

Naming convention and associated compositions.

Naming Convention	Composition
Base	$\text{Na}_{24}\text{Sb}_8\text{S}_{32}$
Ga-doped	$\text{Na}_{21}\text{Ga}_1\text{Sb}_8\text{S}_{32}$
In-doped	$\text{Na}_{21}\text{In}_1\text{Sb}_8\text{S}_{32}$
Y-doped	$\text{Na}_{21}\text{Y}_1\text{Sb}_8\text{S}_{32}$
Ca-doped	$\text{Na}_{22}\text{Ca}_1\text{Sb}_8\text{S}_{32}$
Ba-doped	$\text{Na}_{22}\text{Ba}_1\text{Sb}_8\text{S}_{32}$

## CHAPTER IV

### PHASE STABILITY OF SELENIUM-DOPED SULFIDE ELECTROLYTE

The content presented in this chapter is published as part of an article in ChemSusChem. [Halacoglu, Selim, Sabina Chertmanova, Yan Chen, Yang Li, Manthila Rajapakse, Gamini Sumanasekera, Badri Narayanan, and Hui Wang]. Studying selenide-doped NSS and how the doping effected phase transitioning from the cubic to tetragonal phase in which, DFT calculations were used to understand energetic differences between the cubic and tetragonal polymorphs of  $\text{Na}_3\text{SbS}_{4-x}\text{Se}_x$  at various doping levels of selenium (Se).  $\text{S}^{2-}$  and  $\text{Se}^{2-}$  both being isovalent, anionic species allowed for selenium to occupy any lattice sites that sulfur (S) atoms reserved.

After running calculations and collecting information, the configurations of Se atom placement(s) which had the lowest cohesive energy for the n-doped level were considered as the most stable lattice sites. Cohesive energy for all possible configurations for the desired Se doping amount,  $x$ , were calculated. 510 possible atomic configurations were evaluated, half of which were for cubic structures and the other half for tetragonal structures. Figure 1 shows all cohesive energies found for doping amount  $x=4$ , and polymorphs.

The correlations found between various doping levels and cohesive energies of the most stable doped structures found within cubic and tetragonal polymorphs along

with the phase transition point that was noted. It is apparent that from ranges in the original unit cell where  $x$  is [0,3] the most stable compositions were found in tetragonal polymorph, whereas unit cell ranges where  $x > 3$  the cubic phase becomes thermodynamically stabilized at high Se doping levels, as seen in Figure 2. It is worthy to also note that the difference between the two phase's energetic difference was relatively low (<40 meV/u.f.) at any given doping level, meaning that the cubic phase could be stabilized at high temperatures.

Furthermore, to confirm the findings, XRD and neutron diffraction experiments were performed which showed the formation of the tetragonal phase taking place at low Se doping and when temperatures rose above 350 °C, the characteristic diffraction peaks appear corresponding to the cubic structure of  $\text{Na}_3\text{SbS}_{3.5}\text{Se}_{0.5}$ . The cubic structure showed stability of the composition until it transitions to molten state at 600 °C [17]. To confirm the experimental findings, XRD simulations were conducted via the use of Visualization for Electronic and Structural Analysis (VESTA) where Cu K-alpha radiation was utilized to retrieve  $2\theta$  diffraction angles and their intensities. This information was then related to find  $d$ , the spacing of crystal planes and analyzed for the crystal planes which were present. Figure 3 shows a representation of the findings from the XRD simulations.

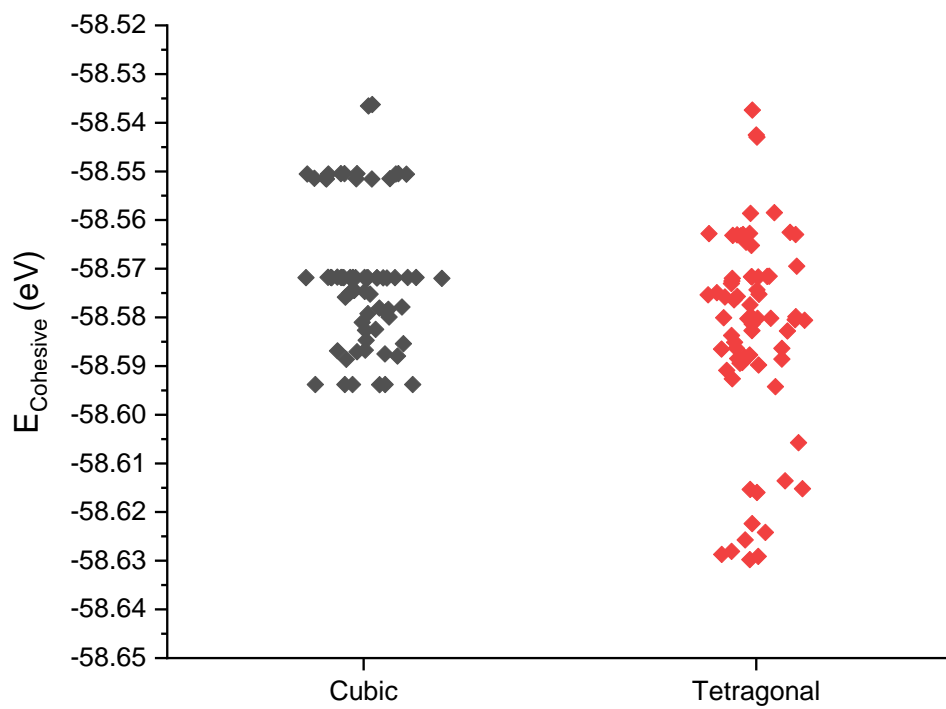


Figure 1. Cohesive energy data points found in all possible combinations of sites that Se can substitute S atoms with  $x=4$  in  $c\text{-Na}_6\text{Sb}_2\text{S}_{8-x}\text{Se}_x$  and  $t\text{-Na}_6\text{Sb}_2\text{S}_{8-x}\text{Se}_x$ .

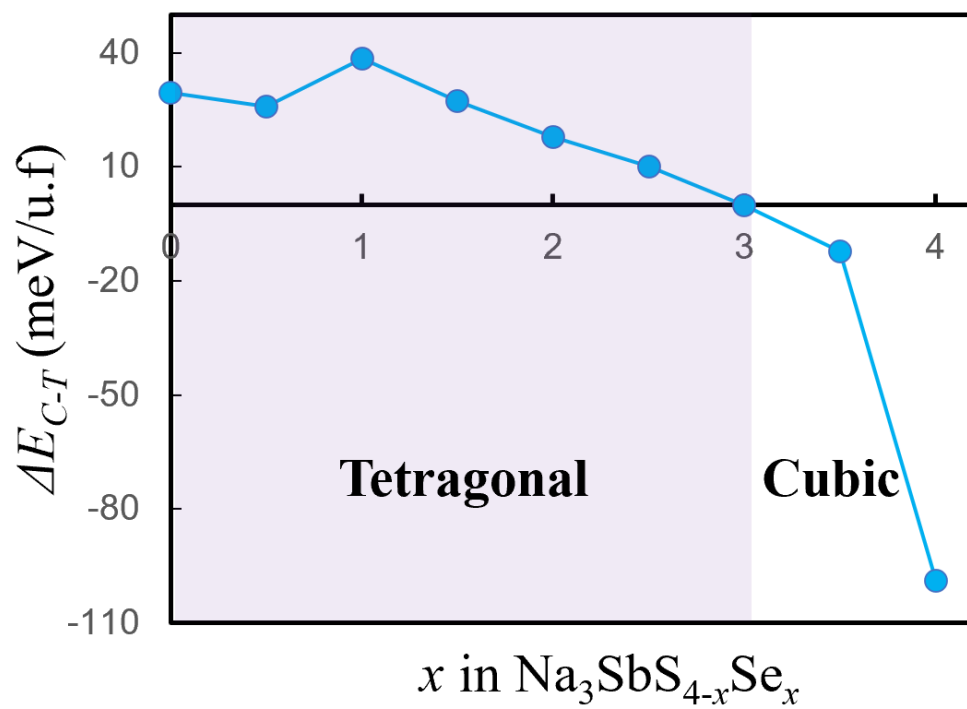
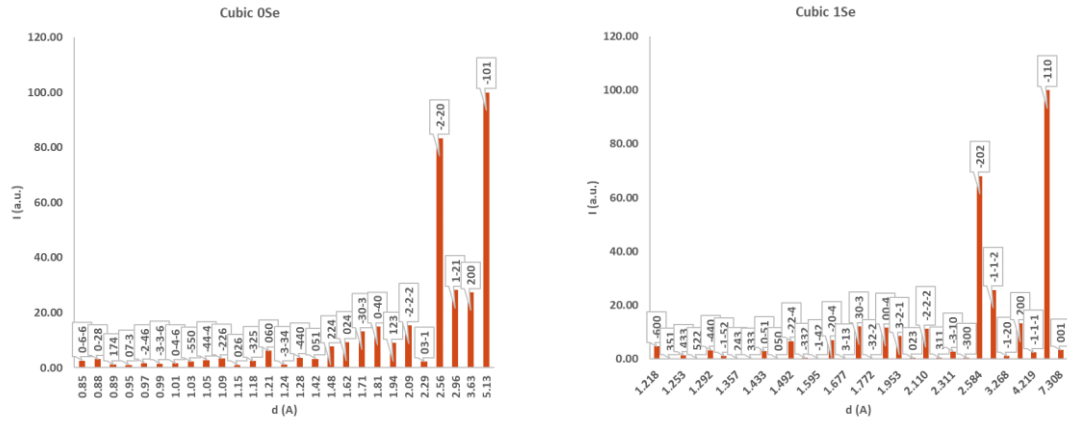
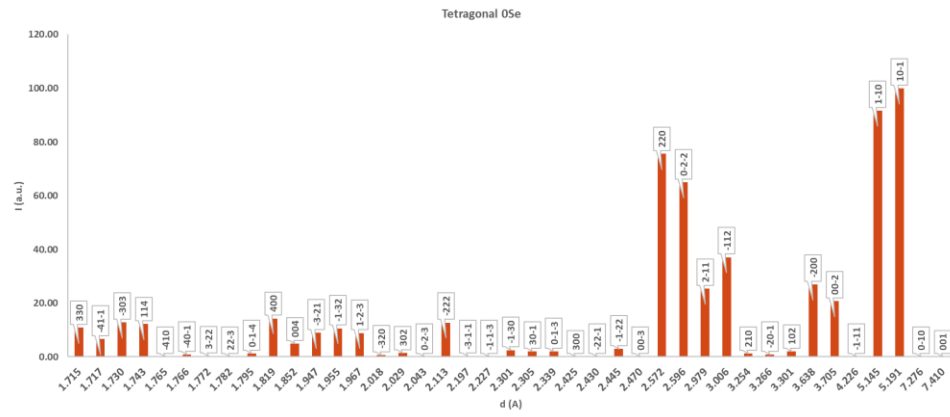


Figure 2. Difference in energies between cubic and tetragonal phases at various levels of Se doping ( $x$ ).

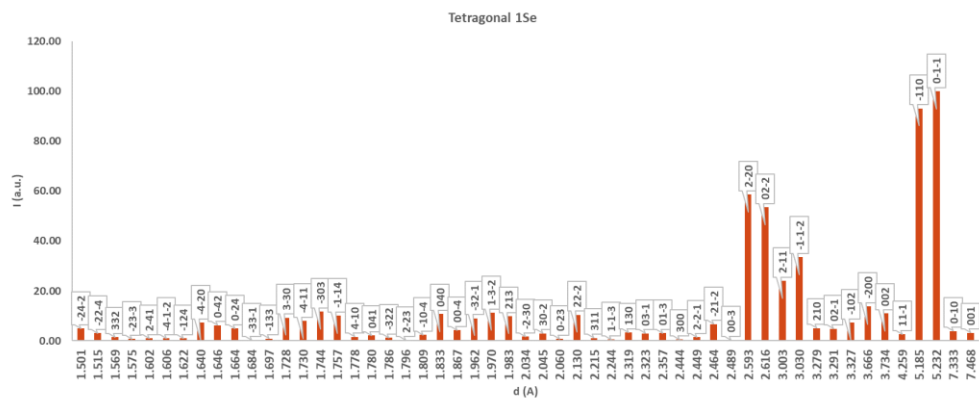


(a)

(b)



(c)



(d)

**Figure 3.** Planar differences in between undoped NSS and single Se-doped NSS in (a-b) Cubic, (c-d) Tetragonal phases.

## CHAPTER V

### EFFECT OF CHEMICAL DOPING ON SODIUM ION CONDUCTION

Once trajectories for each composition from Table 1 were gathered from AIMD calculations, mean square displacements (MSD) were assessed. The MSD plots, as the one shown in Figure 4, were then used to calculate a self-diffusion coefficient of the Na<sup>+</sup> ion,  $D$ , by simplifying the Einstein-Smoluchowski equation to Equation (1).

$$D = \frac{m_{weighted\ avg.}}{6} \quad (1)$$

Where  $m_{weighted\ avg.}$  is the weighted average slope of the linear regions within the MSD plot for a specific temperature. It is important to note that some points which were found to be outliers from MSD plots will not be considered in linear fittings beyond this point.

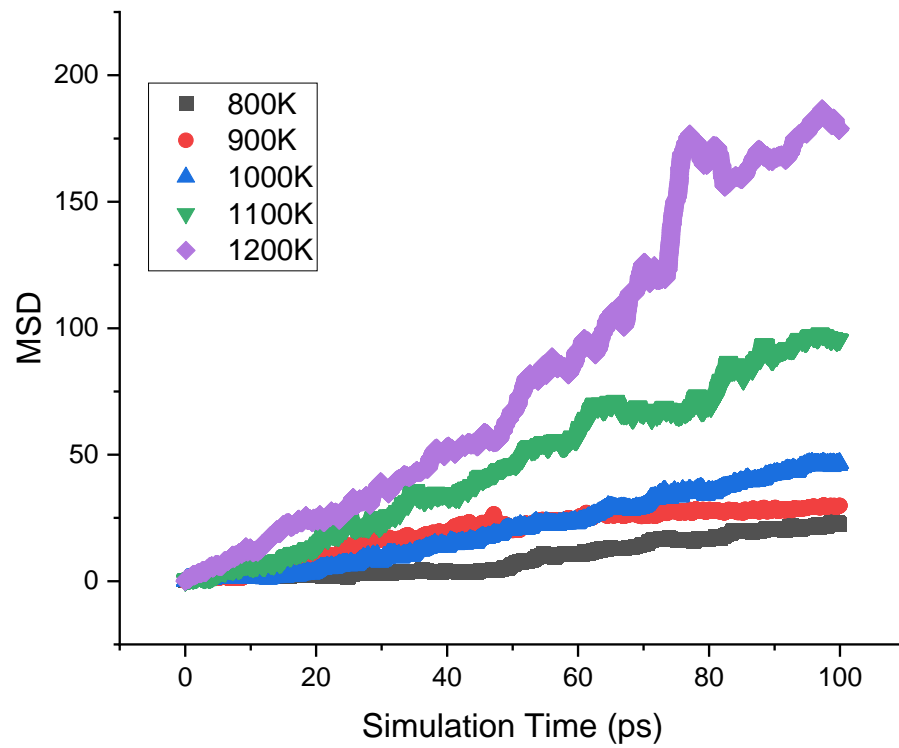


Figure 4. plot of MSD vs. simulation time of c-Ga-doped NSS from 800K-1200K obtained from trajectory files.

The MSD plot shows that with increasing temperatures sodium ions diffuse more over the 100 ps range. Then Arrhenius plots were developed for diffusivity and were fitted linearly, Figures 5-6 show the plots for both cubic and tetragonal crystal structures, respectively. It is apparent that at high temperatures cubic structures dopant compositions, especially those containing In, Ga, Y, have significantly higher diffusivities compared to the Base compound. The Arrhenius plots allowed for the Arrhenius equation to be applied to the diffusion coefficient variable resulting in Equation (2).

$$D = D_0 e^{-\frac{E_a}{RT}} \quad (2)$$

Where  $D_0$  is the pre-exponential factor,  $E_a$  is the activation energy,  $R$  is the gas constant, and  $T$  is the temperature of the system in Kelvin. By algebraically manipulating Equation (2), we can obtain a slope-intercept form of the equation, as seen in Equation (3), which allows us to directly extract activation energies and pre-exponential factors for each composition studied and is presented in Figures 7-8.

$$\log(D) = -2.30258509 \frac{E_a}{R} \left(\frac{1}{T}\right) + \log(D_0) \quad (3)$$

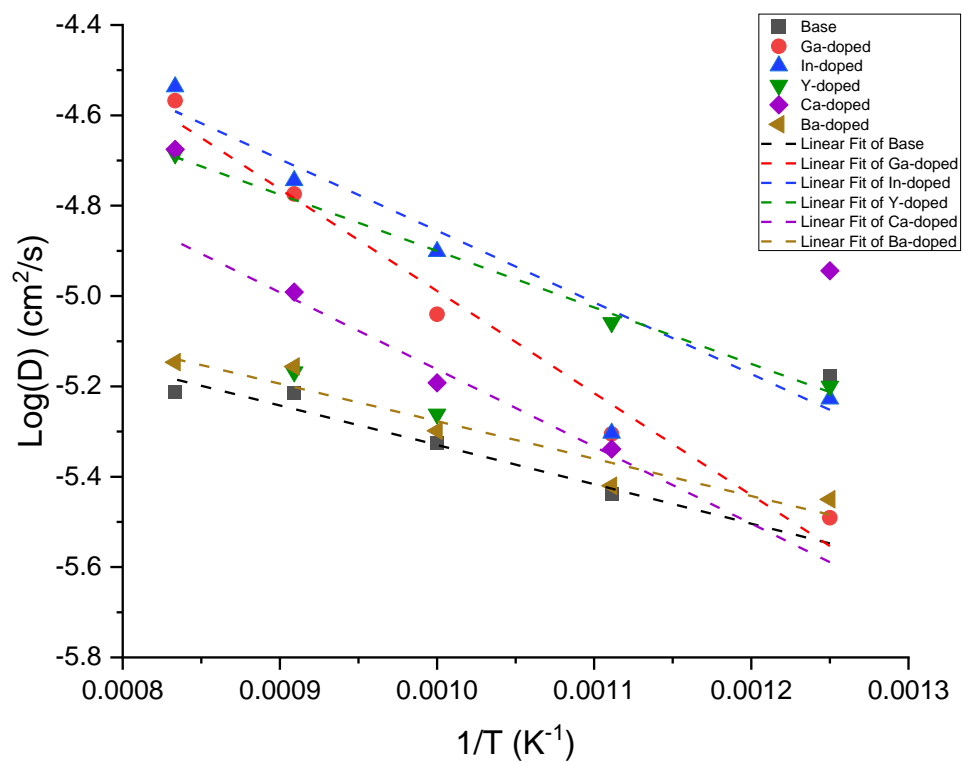


Figure 5. Arrhenius plot of diffusivity for cubic structures.

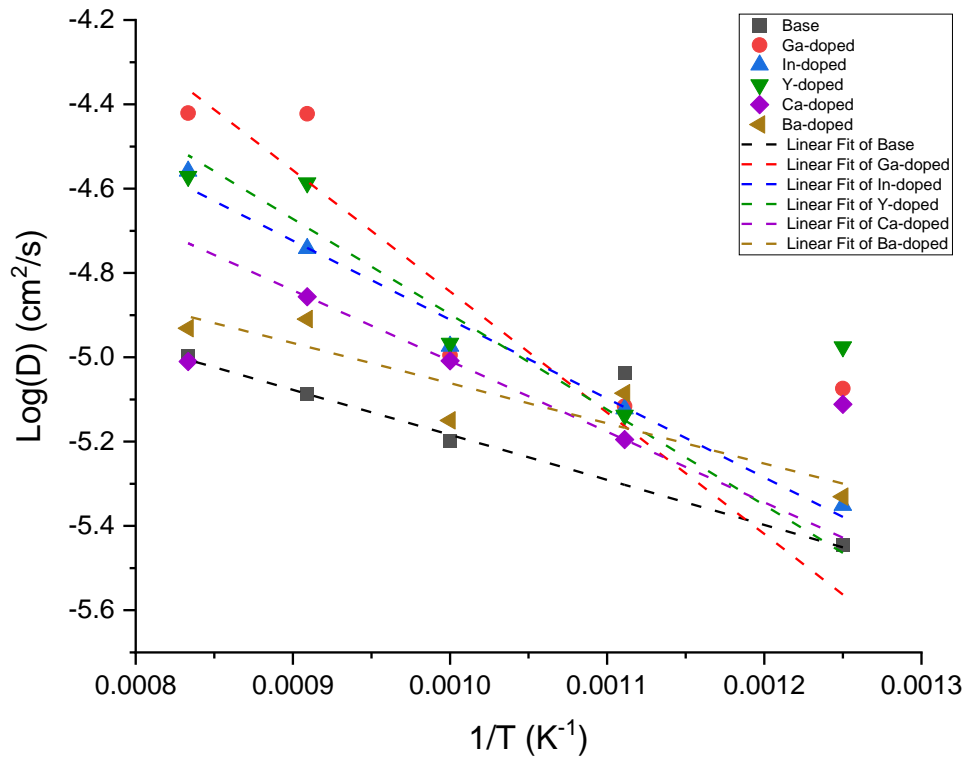


Figure 6. Arrhenius plot of diffusivity for tetragonal structures.

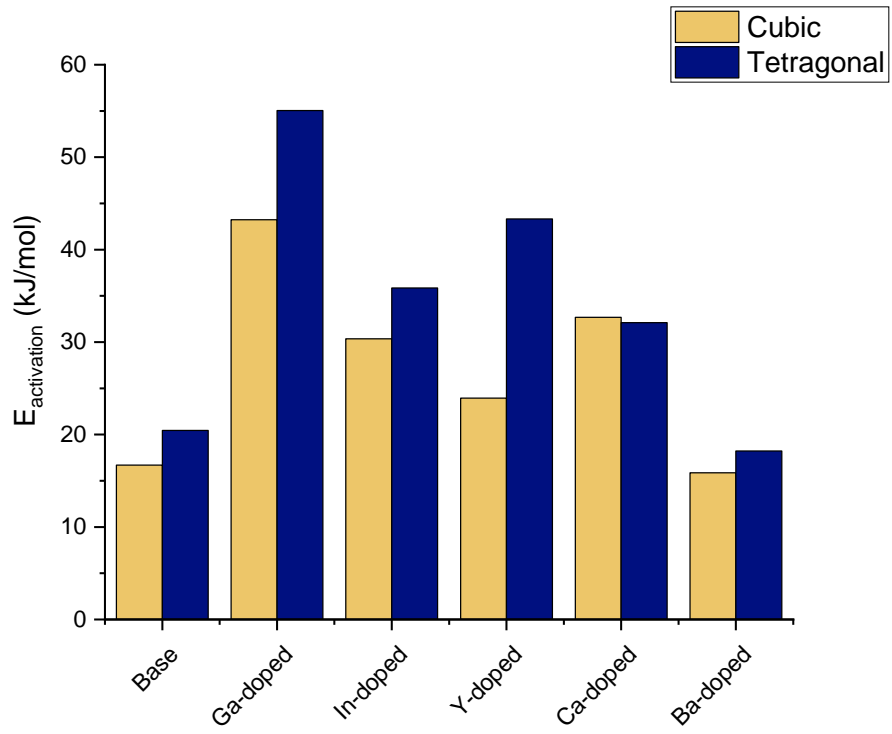


Figure 7. Comparison amongst each composition, polymorph, and corresponding activation energy.

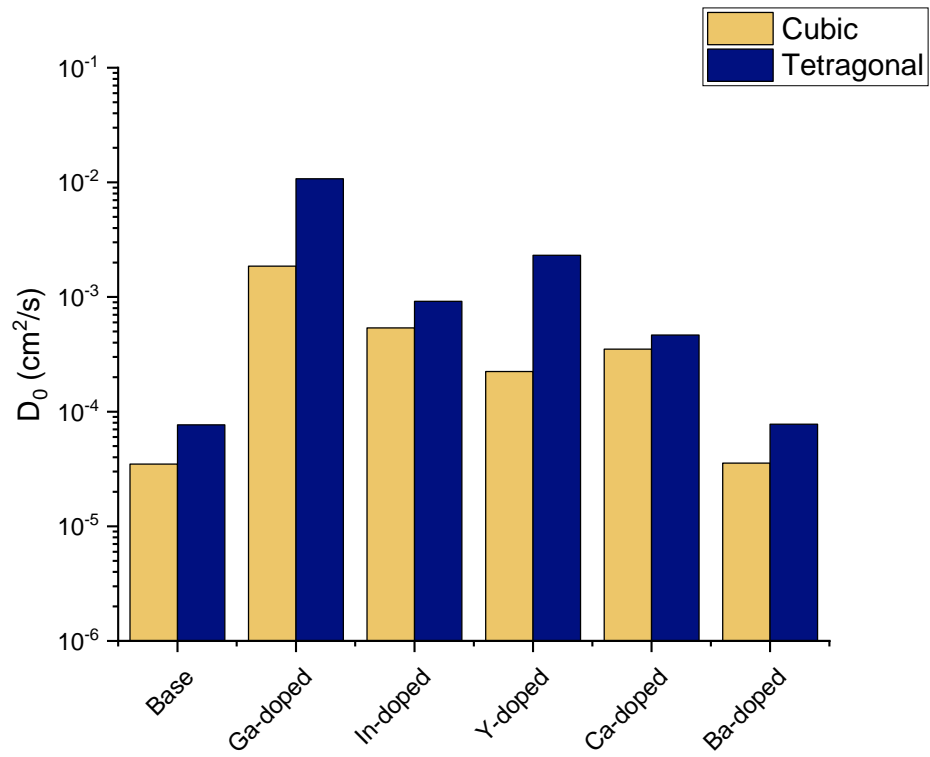


Figure 8. Comparison amongst each composition, polymorph, and corresponding pre-exponential factor.

Though it was hypothesized that increase in diffusivity would lead to decrease of activation energy, we see a clear trend that most doped compounds, though present higher diffusivity compared to the undoped Base, also have higher  $E_a$  and  $D_0$ . Using the Nernst-Einstein equation, ionic conductivity of the sodium ion,  $\sigma$ , was calculated as seen in Equation (4).

$$\sigma = \frac{Nq^2D}{Vk_bT} \quad (4)$$

Where  $N$  is the number of sodium ions present in the system,  $q^2$  is the ion charge associated with  $\text{Na}^+$ ,  $V$  is the volume of the system, and  $k_b$  is the Boltzmann constant. The results of which are shown in Table 2 for reference.

Furthermore, Equation (5) was used to find the formation energies of doped and undoped compositions.

$$E_{form_{composition}} = E_{composition} - \sum_0^i nE_{element} \quad (5)$$

Where  $E_{composition}$  is the total energy associated with a composition,  $i$  is the number of different elements found in said composition,  $n$  is the number of a specific element found in the composition, and  $E_{element}$  is the total energy associated with the relaxation of each element's most stable crystalline structure. The results of which are shown in Figure 9. Finally, to visually observe the diffusivity of sodium ions and what takes place within the interactions of the doped compositions at high temperatures, an open visualization tool (OVITO). OVITO was utilized to aid in tracking a single  $\text{Na}^+$  ion and its mobility throughout the trajectory and how doping affected diffusivity of the sodium ion and its interaction with anionic species.

For context, the initial state of a c-Base composition shows an arrangement of  $\text{SbS}_4^{3-}$  tetrahedrons while simultaneously, the sulfur ions are bonded to a maximum of 5 sodium ions and one antimony. Though the initial layout of t-Base composition is almost the same, the only difference observed is Na ions seem to bond to a maximum of 7 sulfurs. Representations of the Base compositions are shown in Figure 10-11. Furthermore, to gain insight to whether or not temperature effects diffusion pathways c-Base trajectories were observed at 900 K and 1200 K, in which the same exactly  $\text{Na}^+$  ion was selected and tracked. It was noted that temperature does impact diffusion pathways as seen in Figure 12.

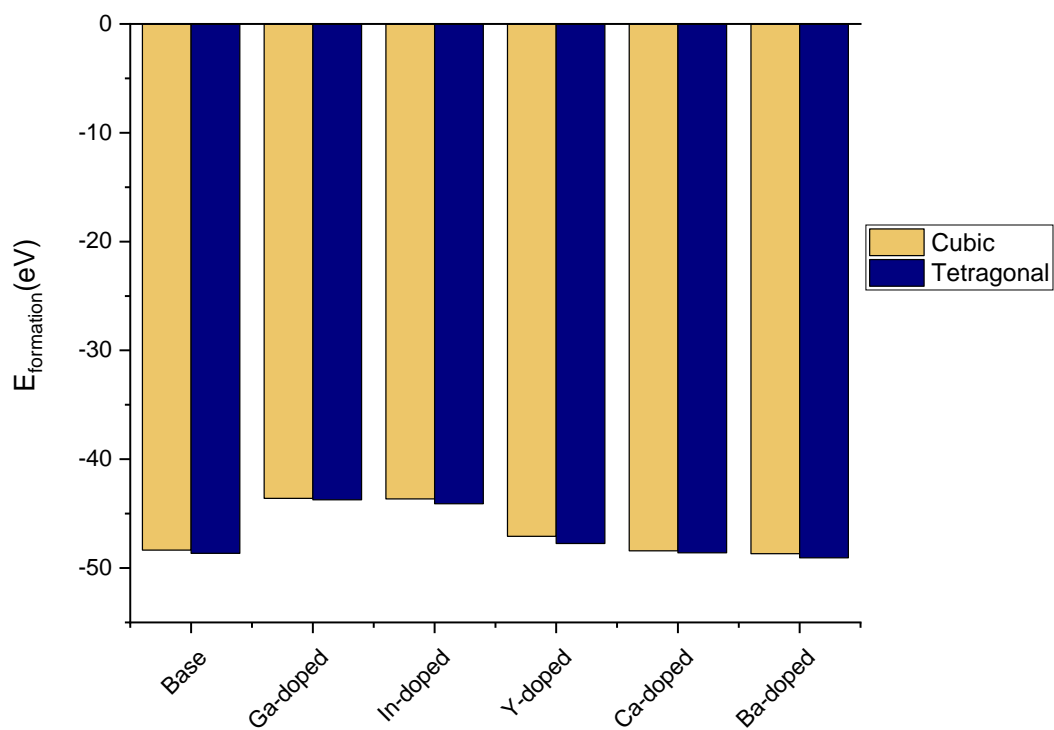
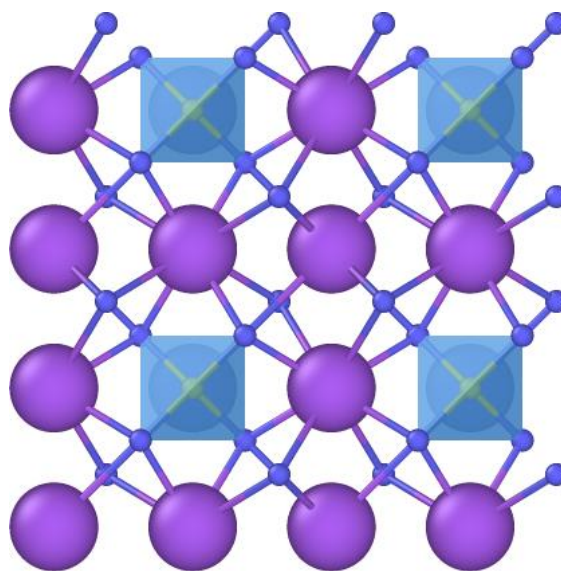
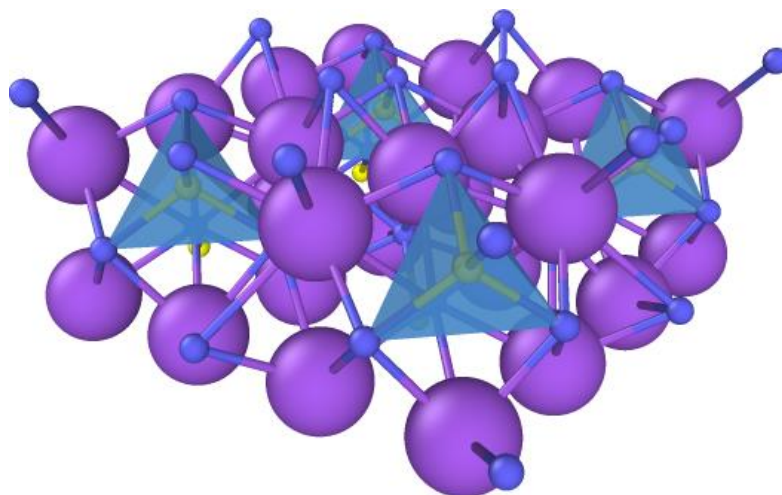


Figure 9. Comparison amongst each composition, polymorph, and corresponding formation energies.

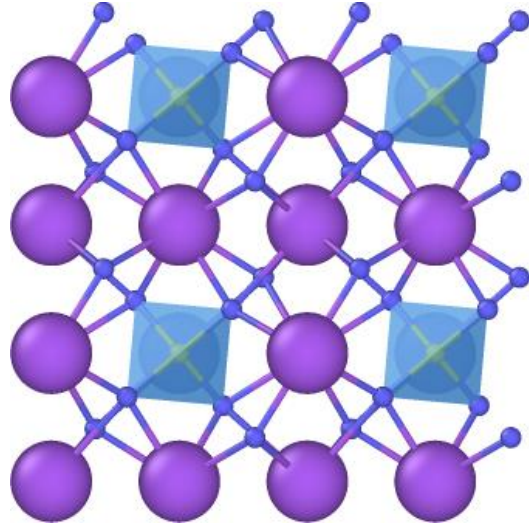


(a)

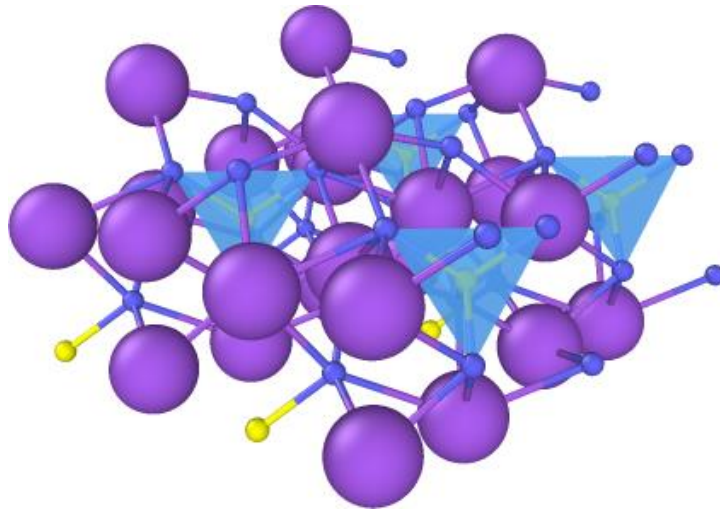


(b)

Figure 10. Ball-and-stick simulation model supercell of c-Based in (a) Top view, (b) Isometric view. Sodium ions, sulfur ions, and antimony ions are seen as purple, blue, and yellow atoms, respectively.



(a)



(b)

Figure 11. Ball-and-stick simulation model supercell of t-Based in (a) Top view, (b) Isometric view. Sodium ions, sulfur ions, and antimony ions are seen as purple, blue, and yellow atoms, respectively.

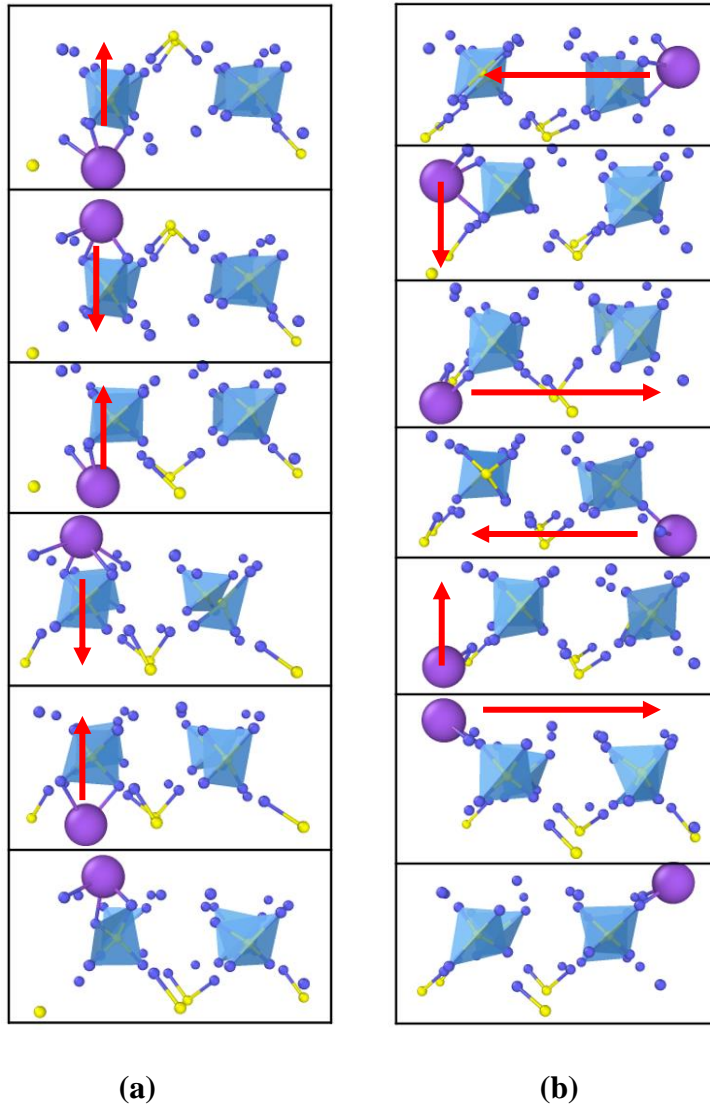


Figure 12. A small portion of sodium diffusion pathways assessed in c-Base at (a) 900 K, (b) 1200 K, via the selection and tracking of same Na ion.

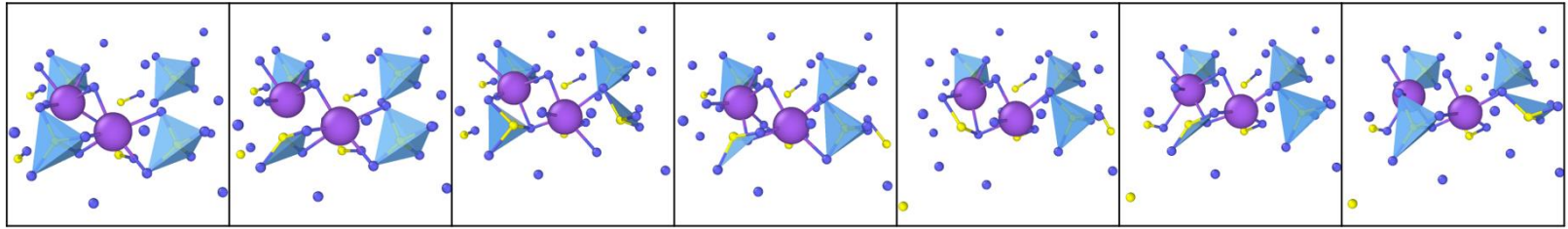
Figures 12-17 show panels of images that were taken in OVITO in sequence over a timeframe, these images contain Na (purple atoms), Sb (yellow atoms), S (blue atoms), and the dopant (green atom) ion. In the cases of sodium ion hops, some images will contain red arrows to distinguish these hops. For Figures 13-17 images in these panels are to be read left-to-right, in sequence, as this is a representation of time progression in the trajectories, meanwhile for Figure 12, images in the panels provided are to be read from top-to-bottom. Some observations that were made during this process are included in the list below along with the figure number where a visual depiction of said observation can be seen.

1. Location of antimony and its proximity to sodium ions is responsible for  $\text{Na}^+$  ion diffusivity in undoped cases, meanwhile, in doped cases, interaction between  $\text{Sb}^{5+}$  and the dopant ion greatly influences sodium ion diffusivity, these two observations are demonstrated in Figure 13. It is apparent that in the undoped case, a trend of  $\text{Na}^+$  ions bonding through a  $\text{SbS}_4$  and then one sodium ion tends to break its bond but still stay in the same site. Meanwhile, in the doped case, we see a trend of a  $\text{Na}^+$  ion and  $\text{Ba}^{2+}$  ion bonding through a  $\text{SbS}_4$  and when the bond to the sodium ion is broken, the sodium ion tends to jump to a different site, in turn, increasing diffusivity of Na.
2. Furthermore, when comparing dopants with oxidation states of 2+ and 3+, c-Ba-doped and c-Ga-doped, the dopant element's charge, and the number of valence sites it creates seems to have a bigger impact on diffusivity compared to electropositivity as seen in Figures 14-15.

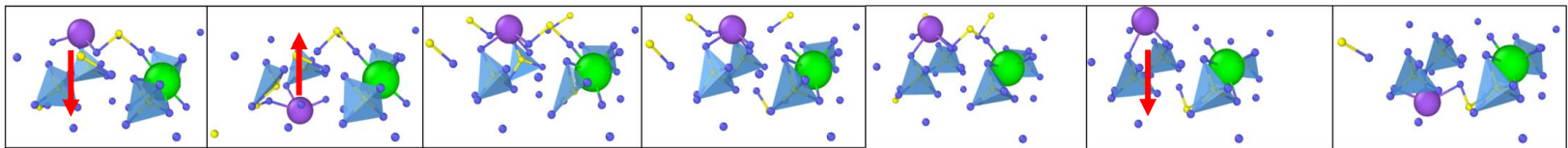
Evidently, we see less  $\text{SbS}_4$  tetrahedrons existing throughout the trajectory and more Na atoms interconnected to each other through sulfur atoms only rather than through an antimony-sulfur bond. On a different note, we see in Ga-doped composition, that whenever Na ions connect to Ga ions through sulfur bond, when this connection is broken, the sulfur tends to stay with the gallium ion while the sodium jumps to a different site.

3. While comparing dopants with same oxidation states and different ionic sizes, in this case  $\text{Ga}^{3+}$  and  $\text{In}^{3+}$ , and there is a suspicion that the interplay between ionic size and electropositivity is what impacts sodium ion diffusivity. This is depicted in Figure 14 and Figure 16.
4. When looking at same dopant compositions with different crystal structure, using c-Ga-doped and t-Ga-doped at 1200 K, Figures 14 and 17 show the two comparisons and it's noted that the tetragonal structure seems to preserve the  $\text{SbS}_4$  tetrahedrons more than the cubic structure does. This results in the connection between antimony and sodium through sulfur bonds. This eventually results in sodium ion hops along with the already noted sodium hops we observed through the connection of Ga and Na ions through sulfur bonds as mentioned in observation number 2.
5. Lastly, cation jumps (sodium or dopant ions) are often symmetric, in the sense that if a cation bonded to 3 sulfur ions will jump across the

simulation cell to a site that will also allow it to be bonded to 3 sulfur ions, most likely to locations with less positively charged ion crowding.

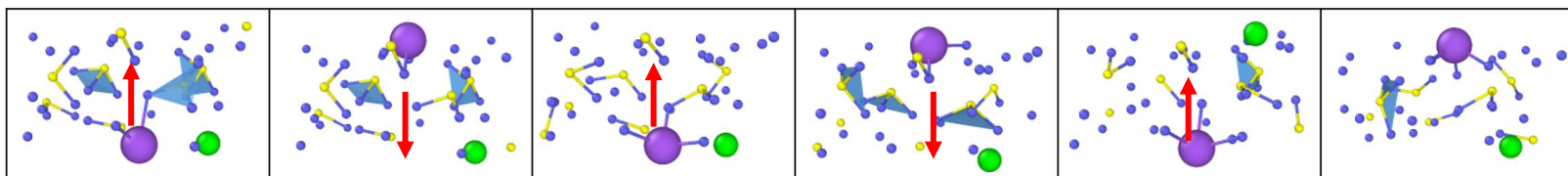


(a)

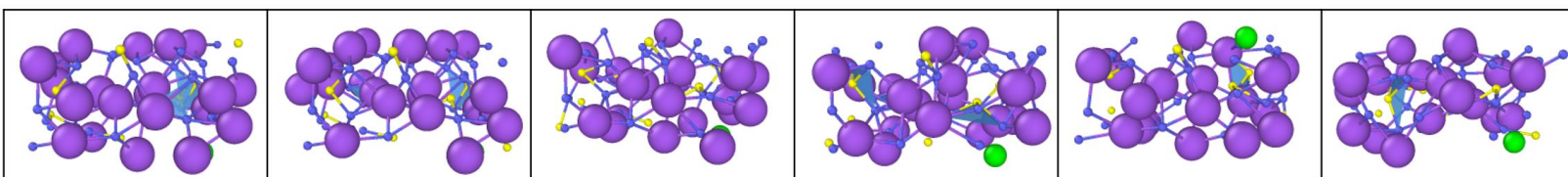


(b)

**Figure 13.** Ball-and-stick visual comparison of (a) c-Base, undoped NSS and (b) c-Ba-doped NSS, and the interaction between  $\text{SbS}_4$  tetrahedron (Sb ions seen in yellow, S ions in blue) and Na-Na ion (purple)/Ba ion (green)-Na ion interactions at 1200 K.

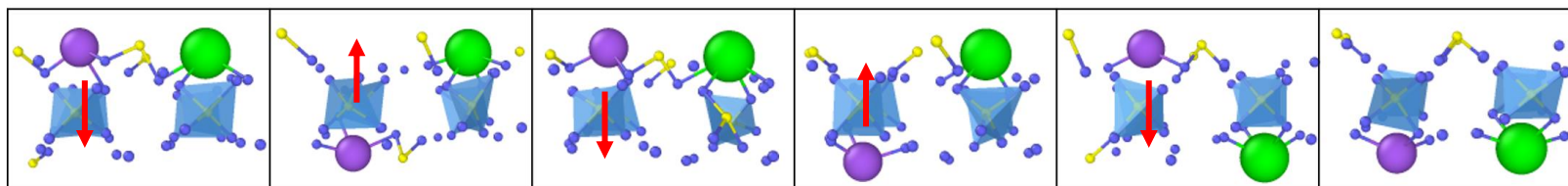


(a)

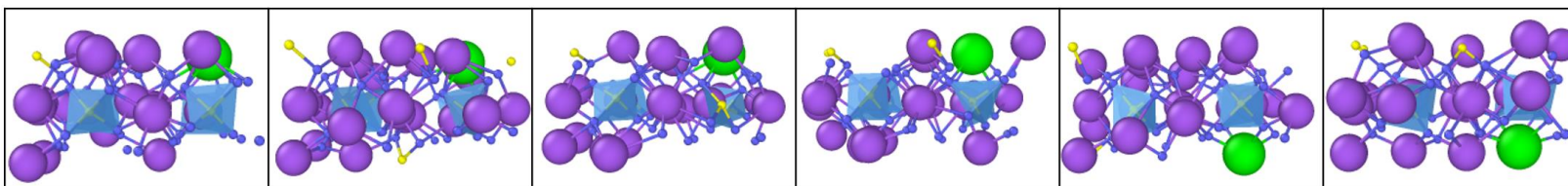


(b)

Figure 14. Ball-and-stick visual representation of c-Ga-doped NSS and the (a) interaction between  $\text{Na}^+$  ion and Ga dopant and (b) corresponding visual images of overall structure and sites that Na occupies, at 1200 K.

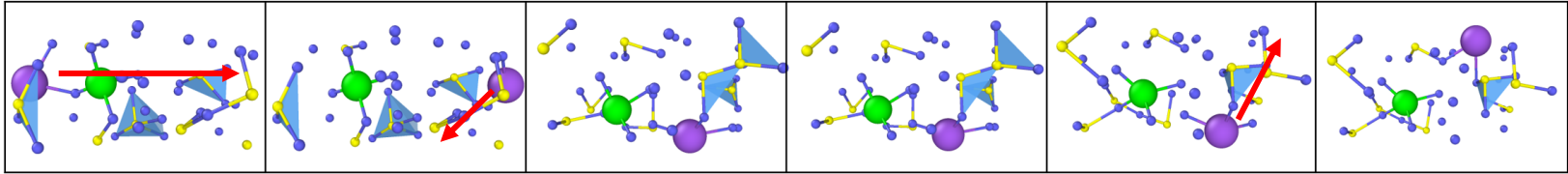


(a)

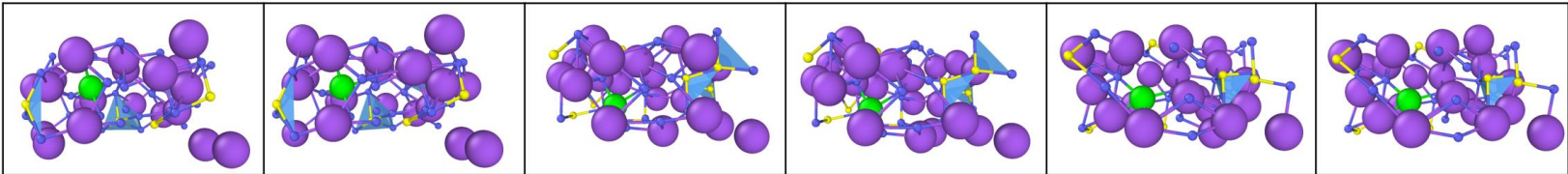


(b)

Figure 15. Ball-and-stick visual representation of c-Ba-doped NSS and the (a) interaction between Na<sup>+</sup> ion and Ba dopant and (b) corresponding visual images of overall structure and sites that Na occupies, at 1200 K.

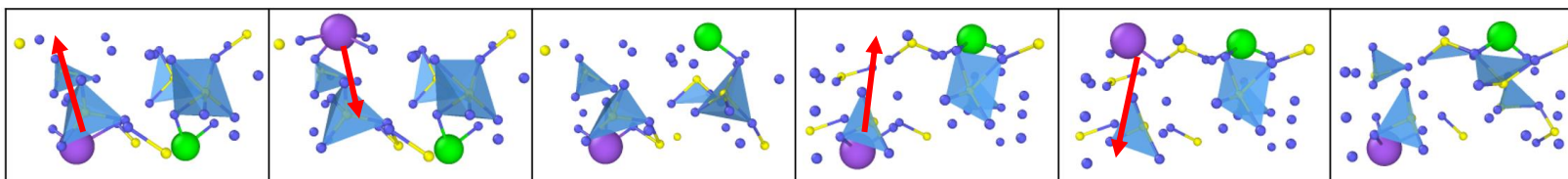


(a)

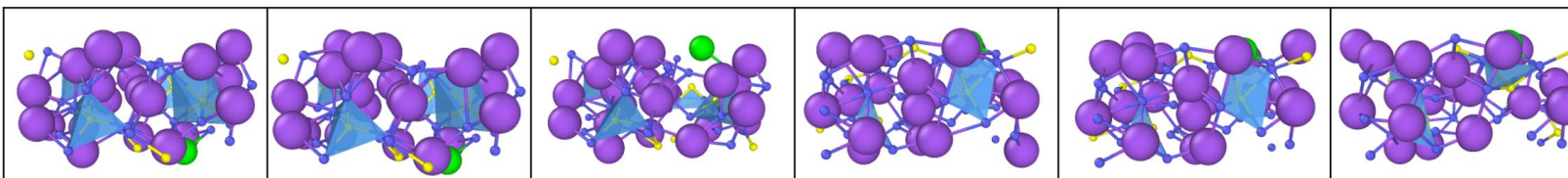


(b)

Figure 16. Ball-and-stick visual representation of c-In-doped NSS and the (a) interaction between  $\text{Na}^+$  ion and In dopant and (b) corresponding visual images of overall structure and sites that Na occupies, at 1200 K.



(a)



(b)

Figure 17. Ball-and-stick visual representation of t-Ga-doped NSS and the (a) interaction between  $\text{Na}^+$  ion and Ga dopant and (b) corresponding visual images of overall structure and sites that Na occupies, at 1200 K.

Though not much NSS related work has been done with every dopant used in this thesis or the high temperatures mentioned, there are some theoretical studies, that the diffusivity findings can be related to if extrapolated to room temperature with additional datapoints. It is important to note that the context of methodology used can greatly impact the results found in simulations. Also, that there is sometimes outlier data that maybe be scrapped leaving insufficient quantities of datapoints to work with which can also have a big impact on findings. With these points in mind, further research needs to be conducted to further confirm the trends found in this thesis.

For reference, Table 2 consists of information about dopant type, charge, electronegativity, and the found sodium diffusivity at 1100 K and the associated conductivity.

**Table 2**

Dopant/ion information and resulting diffusivity and ionic conductivity at 1100 K.

<b>Name</b>	<b>Dopant Ion</b>	<b>Ionic radius (Angstrom)</b>	<b>Electro-negativity</b>	<b><math>D_{1100K}</math> (cm<sup>2</sup>/s)</b>	<b><math>\sigma_{1100K}</math> (mS cm<sup>-1</sup>)</b>
c-Base	N/A	1.16 (Na <sup>+</sup> )	0.93 (Na <sup>+</sup> )	6.12E-06	162.52
c-Ga-doped	Ga <sup>3+</sup>	0.76	1.81	1.68E-05	391.01
c-In-doped	In <sup>3+</sup>	0.94	1.78	1.80E-05	418.78
c-Y-doped	Y <sup>3+</sup>	1.04	1.22	6.79E-06	157.86
c-Ca-doped	Ca <sup>2+</sup>	1.14	1.00	1.02E-05	248.53
c-Ba-doped	Ba <sup>2+</sup>	1.49	0.89	6.98E-06	170.06

Furthermore, the findings in Table 2 are consistent with the observations made at high temperatures through the utilization of trajectories. This includes doped compositions resulting in higher diffusivity and ionic conductivity, an increase in oxidation state in the dopant ion tends to result in increase of  $D$  and  $\sigma$ , there seems to be an interplay between ionic size and electropositivity as we see in the case of c-In-doped and c-Ga-doped.

## CHAPTER VI

### CONCLUSIONS

In conclusion, we see  $\text{Na}_3\text{SbSe}_x\text{S}_{4-x}$  undergo a tetragonal-to-cubic structural phase transition at  $x > 3$ , meanwhile in the second part of this thesis we note that pure NSS's sodium ion conductivity at high temperatures can benefit through the use of dopants with ionic radii smaller than that of sodium ion, lower electropositivity, higher ionic charges, and through utilization of Na vacancies and understanding how increase in higher concentrations of dopants will affect sodium diffusivity. The ion transport pathways play an important role in this study and the interaction of dopant elements and tetrahedron  $\text{SbS}_4$  should be carefully considered.

Though the study was successful it would be of interest for more studies to be done in this area of research to further confirm findings.

## REFERENCES

- [1] Hooper, A. “A Study of the Electrical Properties of Single-Crystal and Polycrystalline  $\beta$ -Alumina Using Complex Plane Analysis.” *Journal of Physics D: Applied Physics*, vol. 10, no. 11, 1977, pp. 1487–96. *Crossref*, doi:10.1088/0022-3727/10/11/013.
- [2] Khireddine, H., et al. “Optimization of NASICON Composition for Na<sup>+</sup> Recognition.” *Sensors and Actuators B: Chemical*, vol. 40, no. 2–3, 1997, pp. 223–30. *Crossref*, doi:10.1016/s0925-4005(97)80266-3.
- [3] Hayashi, Akitoshi, Kousuke Noi, et al. “Superionic Glass-Ceramic Electrolytes for Room-Temperature Rechargeable Sodium Batteries.” *Nature Communications*, vol. 3, no. 1, 2012. *Crossref*, doi:10.1038/ncomms1843.
- [4] Tanibata, Naoto, et al. “Preparation and Characterization of Highly Sodium Ion Conducting Na<sub>3</sub>PS<sub>4</sub>–Na<sub>4</sub>Si<sub>3</sub>S<sub>4</sub> Solid Electrolytes.” *RSC Adv.*, vol. 4, no. 33, 2014, pp. 17120–23. *Crossref*, doi:10.1039/c4ra00996g.
- [5] Zhang, Long, Kun Yang, et al. “Na<sub>3</sub>PSe<sub>4</sub>: A Novel Chalcogenide Solid Electrolyte with High Ionic Conductivity.” *Advanced Energy Materials*, vol. 5, no. 24, 2015, p. 1501294. *Crossref*, doi:10.1002/aenm.201501294.
- [6] Wang, Ning, et al. “Improvement in Ion Transport in Na<sub>3</sub>PSe<sub>4</sub>–Na<sub>3</sub>SbSe<sub>4</sub> by Sb Substitution.” *Journal of Materials Science*, vol. 53, no. 3, 2017, pp. 1987–94. *Crossref*, doi:10.1007/s10853-017-1618-0.
- [7] Duchardt Marc, et al. “Vacancy-Controlled Na<sup>+</sup> Superior Conduction in Na<sub>11</sub>.” *Angewandte Chemie*, vol. 130, no. 5, 2018, pp. 1365–69. *Crossref*, doi:10.1002/ange.201712769.
- [8] Moon, Chang Ki, et al. “Vacancy-Driven Na<sup>+</sup> Superionic Conduction in New Ca-Doped Na<sub>3</sub>PS<sub>4</sub> for All-Solid-State Na-Ion Batteries.” *ACS Energy Letters*, vol. 3, no. 10, 2018, pp. 2504–12. *Crossref*, doi:10.1021/acsenergylett.8b01479.
- [9] Chu, Iek-Heng, et al. “Room-Temperature All-Solid-State Rechargeable Sodium-Ion Batteries with a Cl-Doped Na<sub>3</sub>PS<sub>4</sub> Superionic Conductor.” *Scientific Reports*, vol. 6, no. 1, 2016. *Crossref*, doi:10.1038/srep33733.

- [10] Wang, Hui, et al. “An Air-Stable Na<sub>3</sub>SbS<sub>4</sub> Superionic Conductor Prepared by a Rapid and Economic Synthetic Procedure.” *Angewandte Chemie*, vol.128, no. 30, 2016, pp. 8693–97. *Crossref*, doi:10.1002/ange.201601546.
- [11] Banerjee, Abhik, et al. “Na<sub>3</sub>SbS<sub>4</sub>: A Solution Processable Sodium Superionic Conductor for All-Solid-State Sodium-Ion Batteries.” *Angewandte Chemie*, vol. 128, no. 33, 2016, pp. 9786–90. *Crossref*, doi:10.1002/ange.201604158.
- [12] Zhang, Long, et al. “Vacancy-Contained Tetragonal Na<sub>3</sub>SbS<sub>4</sub> Superionic Conductor.” *Advanced Science*, vol. 3, no. 10, 2016, p. 1600089. *Crossref*, doi:10.1002/advs.201600089
- [13] Hayashi, A., et al. “A Sodium-Ion Sulfide Solid Electrolyte with Unprecedented Conductivity at Room Temperature.” *Nature Communications*, vol. 10, no. 1, 2019. *Crossref*, doi:10.1038/s41467-019-13178-2.
- [14] Hayashi, Akitoshi, et al. “Development of Sulfide Solid Electrolytes and Interface Formation Processes for Bulk-Type All-Solid-State Li and Na Batteries.” *Frontiers in Energy Research*, vol. 4, 2016. *Crossref*, doi:10.3389/fenrg.2016.00025.
- [15] Zhou, Chengtian, et al. “Engineering Materials for Progressive All-Solid-State Na Batteries.” *ACS Energy Letters*, vol. 3, no. 9, 2018, pp. 2181–98. *Crossref*, doi:10.1021/acsenergylett.8b00948.
- [16] Jalem, Randy, et al. “First-Principles Calculation Study of Na<sup>+</sup> Superionic Conduction Mechanism in W- and Mo-Doped Na<sub>3</sub>SbS<sub>4</sub> Solid Electrolytes.” *Chemistry of Materials*, vol. 32, no. 19, 2020, pp. 8373–81. *Crossref*, doi:10.1021/acs.chemmater.0c02318.
- [17] Halacoglu, Selim, et al. “Visualization of Solid-State Synthesis for Chalcogenide Na Superionic Conductors by In-situ Neutron Diffraction.” *ChemSusChem*, 2021. *Crossref*, doi:10.1002/cssc.202101839.
- [18] Wan, Hongli, et al. “Bio-Inspired Nanoscaled Electronic/Ionic Conduction Networks for Room-Temperature All-Solid-State Sodium-Sulfur Battery.” *Nano Today*, vol. 33, 2020, p. 100860. *Crossref*, doi:10.1016/j.nantod.2020.100860.
- [19] Klerk, Niek J. J. de, and Marnix Wagemaker. “Diffusion Mechanism of the Sodium-Ion Solid Electrolyte Na<sub>3</sub>PS<sub>4</sub> and Potential Improvements of Halogen Doping.” *Chemistry of Materials*, vol. 28, no. 9, 2016, pp. 3122–30. *Crossref*, doi:10.1021/acs.chemmater.6b00698.
- [20] Gamo, Hirotada, et al. “Multiphase Na<sub>3</sub>SbS<sub>4</sub> with High Ionic Conductivity.” *Materials Today Energy*, vol. 13, 2019, pp. 45–49. *Crossref*, doi:10.1016/j.mtener.2019.04.012.

- [21] Zhang, Qian, et al. “Abnormally Low Activation Energy in Cubic Na<sub>3</sub>SbS<sub>4</sub> Superionic Conductors.” *Chemistry of Materials*, vol. 32, no. 6, 2020, pp. 2264–71. *Crossref*, doi:10.1021/acs.chemmater.9b03879.
- [22] Xiong, Shan, et al. “Na<sub>3</sub>SbSe<sub>4-x</sub>S<sub>x</sub> as Sodium Superionic Conductors.” *Scientific Reports*, vol. 8, no. 1, 2018. *Crossref*, doi:10.1038/s41598-018-27301-8.
- [23] Wan, Hongli, Jean Pierre Mwizerwa, et al. “Grain-Boundary-Resistance-Less Na<sub>3</sub>SbS<sub>4</sub>-Se Solid Electrolytes for All-Solid-State Sodium Batteries.” *Nano Energy*, vol. 66, 2019, p. 104109. *Crossref*, doi:10.1016/j.nanoen.2019.104109.
- [24] Cao, Haonan, et al. “Stabilizing Na<sub>3</sub>SbS<sub>4</sub>/Na Interface by Rational Design via Cl Doping and Aqueous Processing.” *Journal of Materials Science & Technology*, vol. 70, 2021, pp. 168–75. *Crossref*, doi:10.1016/j.jmst.2020.08.035.
- [25] Park, Kern Ho, et al. “Solution-Derived Glass-Ceramic NaI·Na<sub>3</sub>SbS<sub>4</sub> Superionic Conductors for All-Solid-State Na-Ion Batteries.” *Journal of Materials Chemistry A*, vol. 6, no. 35, 2018, pp. 17192–200. *Crossref*, doi:10.1039/c8ta05537h.

## APPENDIX

### JOHN WILEY AND SONS LICENSE TERMS AND CONDITIONS

Dec 03, 2021

---

---

This Agreement between University of Louisville -- Sabina Chertmanova ("You") and John Wiley and Sons ("John Wiley and Sons") consists of your license details and the terms and conditions provided by John Wiley and Sons and Copyright Clearance Center.

License Number 5201460591768

License date Dec 03, 2021

Licensed  
Content  
Publisher John Wiley and Sons

Licensed  
Content  
Publication ChemSusChem

Licensed  
Content Title Visualization of Solid-State Synthesis for Chalcogenide Na Superionic  
Conductors by in-situ Neutron Diffraction

Licensed  
Content Author Selim Halacoglu, Sabina Chertmanova, Yan Chen, et al

Licensed  
Content Date Nov 5, 2021

Licensed  
Content Volume 0

Licensed  
Content Issue 0

Licensed  
Content Pages 1

Type of use	Dissertation/Thesis
Requestor type	Author of this Wiley article
Format	Electronic
Portion	Figure/table
Number of figures/tables	2
Will you be translating?	No
Title	ATOMISTIC INVESTIGATION OF PHASE STABILITY AND SODIUM ION CONDUCTION IN SULFIDE ELECTROLYTES
Institution name	University of Louisville
Expected presentation date	Dec 2021
Portions	Figures related to DFT computations and analysis  University of Louisville
Requestor Location	LOUISVILLE, KY 40215 United States Attn: University of Louisville
Publisher Tax ID	EU826007151
Total	0.00 USD

## CURRICULUM VITA

NAME: Sabina Zakhidovna Chertmanova  
ADDRESS: Department of Mechanical Engineering  
2301 S. Third St.  
University of Louisville  
Louisville, KY 40208  
DOB: Rostov-on-Don, Russia – July 5, 1997

### EDUCATION

& TRAINING: B.S., Mechanical Engineering  
University of Louisville  
2016-20  
M.S., Mechanical Engineering  
University of Louisville  
2020-21

### PUBLICATIONS:

Halacoglu, Selim, Sabina Chertmanova, Yan Chen, Yang Li, Manthila Rajapakse, Gamini Sumanasekera, Badri Narayanan, and Hui Wang. "Visualization of Solid-State Synthesis for Chalcogenide Na Superionic Conductors by in-situ Neutron Diffraction." *ChemSusChem* (2021).

### NATIONAL MEETING PRESENTATIONS:

Zhang, Shanshan, Sabina Chertmanova, and Kevin Chou. "Surrogate Pore Generations in L-PBF Ti64 and Effects on Mechanical Behavior." *International Manufacturing Science and Engineering Conference*. Vol. 84256. American Society of Mechanical Engineers, 2020.